Palladium clusters confined in triazinyl-functionalized COFs with enhanced catalytic activity

Mengying Fan[a], Wei David Wang[a], Yangyang Zhu[a], Xun Sun[b], Fengwei Zhang[c], Zhengping Dong[a,*]

[a] *State Key Laboratory of Applied Organic Chemistry, Laboratory of Special Function Materials and Structure Design of the Ministry of Education, College of Chemistry and Chemical Engineering, Lanzhou University, Lanzhou 730000, PR China*
[b] *Shandong Applied Research Center of Gold Nanotechnology (Au-SDARC), School of Chemistry & Chemical Engineering, Yantai University, Yantai 264005, PR China*
[c] *Institute of Crystalline Materials, Shanxi University, Taiyuan 030006, PR China*

ARTICLE INFO

ABSTRACT

Noble-metal-cluster-based catalysts have attracted immense research attention due to their high atom utilization ratio and superior catalytic activity. However, it is still challenging to control the size growth of noble-metal clusters. Here, triazinyl-functionalized covalent organic frameworks (Triazinyl-COFs) with different pore diameters were synthesized by the condensation of cyanuric chloride with each of p-phenylenediamine and 4,4′-diaminobiphenyl, referred to as COF-Ph and COF-BPh, respectively. A simple synthetic strategy was employed for controlling the Pd clusters growth and anchoring Pd clusters based on the confinement effect of Triazinyl-COFs pores. The as-obtained Pd@COF-Ph and Pd@COF-BPh catalysts with a Pd cluster size of ˜0.8 nm exhibited superior activity and excellent stability for the reduction of 4-nitrophenol, attributing to the high utilization of Pd active sites and the confinement effect of Triazinyl-COFs. Besides, the influence of the different pore sizes of COF-Ph and COF-BPh on the catalytic performance of the obtained catalysts was also investigated.

1. Introduction

Heterogeneous catalysts exhibit several advantages over homogeneous catalysts, including high recyclability, facile recovery from a reaction mixture, and their facile use in continuous flow processes [1–3]. Metal nanoparticles (NPs) are the ideal choice for the fabrication of supported heterogeneous catalysts due to their excellent properties such as a high surface area and a narrow size distribution [4–6]. Metal clusters, constituting special metal particles with a particle size less than that of metal NPs, have attracted immense research attention in heterogeneous catalysis due to their high atom utilization that can provide more active sites [7,8]. However, the instability caused by the high surface energy of metal clusters always leads to their severe aggregation to metal NPs, subsequently limiting their applications in heterogeneous catalysis. Typically, ligand stabilization [9,10] and matrix supports are employed to improve the stability of metal clusters [11–14]. Nevertheless, by ligand stabilization, the reactants in the catalytic reaction easily exchange with the metal cluster ligands, leading to the decomposition of metal clusters. In contrast, the use of solid supporting materials with heteroatoms, which can provide a coordination environment for metal clusters, is ideal for the fabrication of metal-cluster-based catalysts. In this case, the role of supporting materials may be related to the electron interactions between the supports and metal clusters, as well as to the confinement effect of the supporting material pores [7,14,15]. Hence, it is crucial to design and synthesize supporting materials for the confinement and stabilization of metal clusters with precise topological and abundantly functionalized heteroatom groups.

Meanwhile, covalent organic frameworks (COFs) are typically characterized by the geometry and size of the controllable components to guide the periodic topological evolution of the structure [16–20]. First, compared to other porous materials, COFs exhibit a clear, predictable two- or three-dimensional pore structure, thereby limiting the growth and agglomeration of metal clusters; second, the pores are well separated, thereby reducing the aggregation of embedded metal clusters; the chemical structure of COFs was custom-made in advance, and N,S-rich heterocyclic COFs can effectively anchor metal clusters; a majority of COFs exhibit structural stability as well as excellent stability in various acidic–alkaline reaction media [21]. Several studies have reported excellent stability for various metal NPs that use COFs for stabilization, including Pt and Pd NPs, indicative of the possibility of encapsulation of metal clusters in the COF channels. The encapsulation

and seed growth of metal atoms in the pores are the most crucial factors that limit the growth of metal clusters. On the other hand, in the initial design of COFs, the pore size can be determined on the basis of the synthesized components [22,23]. The abundant, ordered in-plane pores in 2D-COF nanosheets are crucial for the rapid, effective mass transfer of reaction substrates. Hence, COFs serve as an ideal support for improving the stability and recyclability of metal cluster catalysts. Therefore, it is imperative to design and fabricate COFs materials with N atom- or S atom-based groups in the pores for metal-cluster-based catalyst fabrication.

In this study, *p*-phenylenediamine and 4,4′-diaminobiphenyl with different molecular sizes are selected for reaction with cyanuric chloride to afford triazinyl-COFs with different pore sizes, referred to as COF-Ph and COF-BPh, respectively. These two COFs exhibit extremely high stability in acidic and alkaline media as well as in triazinyl-group-doped hydrophilic pores, the distribution experiment of COF-Ph and COF-BPh in *n*-hexane-water system indicates that the two COFs with hydrophobic surface exhibit poor dispersibility in water. Hence, a small amount of a precursor $PdCl_2$ aqueous solution (the volume is less than the pore volume of the adsorbent) can enter the hydrophilic pores due to capillary forces in an organic solvent. The $PdCl_2$ absorbed in the COFs pores is then reduced by a $NaBH_4$ solution, affording Pd@COF-Ph and Pd@COF-BPh catalysts, wherein the Pd clusters are anchored in the COFs pores. The above method is known as the double solvent method (DSM). The obtained Pd clusters catalysts exhibited extremely high catalytic activity and excellent stability for the reduction of nitroaromatic compounds. In addition, the pore size effects of COF-Ph and COF-BPh on the catalytic performance is investigated. This study should provide a useful strategy for the fabrication of noble-metal-cluster-based catalysts for various applications.

2. Experimental

2.1. Materials

Cyanuric chloride (98%), *p*-phenylenediamine (99%), 4,4′-diaminobiphenyl (99%) and palladium chloride ($PdCl_2$, 99%) were purchased from Tianjin Heowns Biochemical Technology Co., Ltd. 4-nitrophenol (4-NP), dioxane, ethanol, dichloromethane and other nitro compounds used in the experiment were obtained from Rionlon Chemical Company. Distilled water was used throughout the whole experiments.

2.2. Synthesis of COF-Ph and COF-BPh

First, a solution of cyanuric chloride (4 mmol) in anhydrous dioxane (20 mL) was slowly added into *p*-phenylenediamine (6 mmol) in anhydrous dioxane (20 mL) in the presence of K_2CO_3 (12 mmol) and subjected to ultrasonication for 30 min. Second, the suspension was added in an oil bath at 90 °C for 72 h. The purple solid was isolated by filtration and washed with dichloromethane, ethanol, and distilled water and extracted using anhydrous dichloromethane for 72 h, followed by drying at room temperature under vacuum, affording COF-Ph. COF-BPh was prepared by the same method using 4,4′-diaminobiphenyl and cyanuric chloride as the starting materials.

2.3. Fabrication of Pd@COF-Ph and Pd@COF-BPh

Typically, the DSM method was employed. First, COF-Ph (50 mg) was suspended in 50 mL of *n*-hexane as the hydrophobic solvent, and 0.05 mL of aqueous $PdCl_2$ (Pd content: 12 mg mL^{-1}) was added dropwise under vigorous stirring. Second, after rotation to dryness, the obtained solid was dispersed in an ethanol solution and reduced using the $NaBH_4$ solution. Pd@COF-Ph was collected by filtration and washed with ethanol and water, and vacuum dried. The Pd@COF-BPh catalyst was prepared by the same method.

2.4. Catalytic activities investigation of Pd@COF-Ph and Pd@COF-BPh

As-prepared Pd@COF-Ph and Pd@COF-BPh were used in the catalytic reduction of 4-NP to 4-AP and reduction of other nitroaromatic compounds by $NaBH_4$. Typically, 30 μL of aqueous 4-NP (0.01 M) and 10 μL of an aqueous catalyst dispersion (10 mg mL^{-1}) were added into 2.5 mL of water, followed by the addition of 0.25 mL of aqueous $NaBH_4$ (0.19 M). The reaction was started, and the progress was monitored by an ultraviolet–visible (UV–vis) spectrophotometer. Mordant Green 17 (MG-17) with large molecule size was also reduced under the same reaction conditions as 4-NP to study the pore size effect. We built these two molecular models and the molecule size of 4-NP and MG-17 are 6.4 Å × 2.4 Å and 7.2 Å × 14.0 Å, respectively (Fig. S1).

In addition, the reduction of other nitro compounds was utilized to investigate the general applicability of Pd@COF-Ph and Pd@COF-BPh catalysts. Generally, 1 mmol of nitrobenzene, 10 mg of catalysts, 1.2 mmol of $NaBH_4$, and 5 mL of solvent were added into a reaction tube. After the reaction was completed, the catalysts were separated and washed with ethanol and water and reused for the next cycle. The reaction mixture was extracted using ethyl acetate and subjected to gas chromatography–mass spectroscopy (GC–MS).

2.5. Characterization

Fourier transform infrared (FTIR) spectroscopy was used to confirm the successful preparation of COF-Ph and COF-BPh. X-ray diffraction (XRD) patterns were recorded on a Rigaku D/max-2400 X-ray diffractometer with monochromatic Cu-Kα radiation in the 2θ range of 5°–90°. Scanning electron microscopy (SEM) images were recorded on an Ultra55 SEM instrument at an accelerating voltage of 20 kV. Transmission electron microscopy (TEM) and energy-dispersive X-ray spectrometry (EDX) were employed to investigate the catalyst structure, morphology, and metal cluster size. Inductively coupled plasma atomic emission spectroscopy (ICP-AES) and elemental microanalysis (EA) were employed to analyze the content of C, N, H, and Pd. Thermogravimetric analysis (TGA) curves of COF-Ph and COF-BPh samples were recorded under N_2 at a ramping rate of 10 °C min^{-1}. X-ray photoelectron spectroscopy (XPS) profiles were recorded on a Perkin-Elmer PHI-5702 electron spectrometer. Brunauer–Emmett–Teller (BET) measurements were carried out on a Micromeritics ASAP 2010 instrument. The reduction of 4-NP and MG-17 was detected by UV–vis spectroscopy. The reduction of nitro compounds was examined by GC–MS (Agilent 5977E).

3. Results and discussion

3.1. Characterization of Pd@COF-Ph and Pd@COF-BPh

Scheme 1 shows the synthesis of Pd@COF-Ph and Pd@COF-BPh. The distribution experiments of COF-Ph and COF-BPh in *n*-hexane-water system shows that COF-BPh and COF-Ph are mainly distributed in *n*-hexane phase (Fig. S2), thus their surface is hydrophobic. The Pd@COF-Ph and Pd@COF-BPh catalysts prepared by the simple DSM method, which involves the accurate introduction of Pd clusters into the COF channel via the utilization of the difference in the hydrophobic surface and hydrophilic pores, while the N atoms of triazinyl-COFs can effectively anchor the metal clusters, and the confinement effect of COF pores can control the Pd cluster growth, thereby obtaining Pd cluster-based catalysts that exhibit high atom utilization and high stability.

To reveal the different between Pd@COF-Ph and Pd@COF-BPh, various characterization tests were conducted. SEM images of COF-Ph, COF-BPh, Pd@COF-Ph, and Pd@COF-BPh (Figs. S3 and 1 a) revealed sheet-like morphology. At the same time, the morphologies of Pd@COF-Ph and Pd@COF-BPh were almost unchanged after modification by Pd clusters. TEM images revealed that Pd@COF-Ph and Pd@COF-BPh are multilayer sheet materials, which is consistent with the lamellar features of pristine COF-Ph and COF-BPh (Figs. 1b and S4). TEM images of
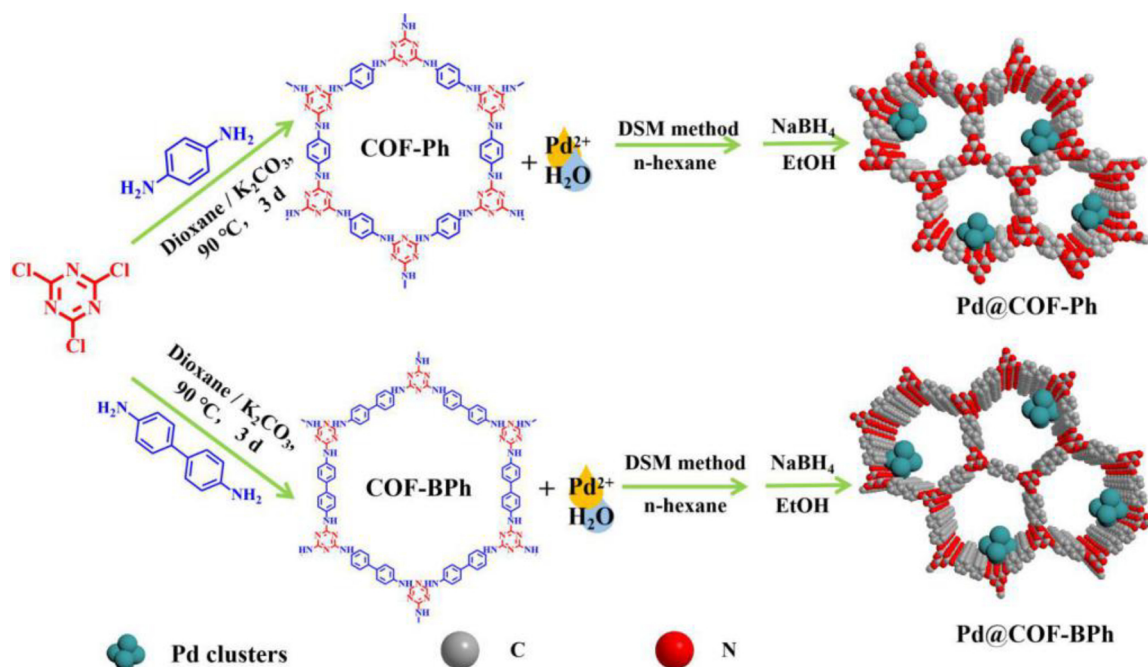
Scheme 1. Synthetic routes of Pd@COF-Ph and Pd@COF-BPh catalysts.

Pd@COF-BPh revealed that the diameter of the Pd clusters ranges from 0.2 to 1.4 nm. Almost all of the Pd clusters are located inside of the COFs pores, and only very few of them are on the surface. Fig. 1c shows the narrow size distribution of the Pd clusters with an average size of 0.81 nm were highly dispersed in the COF-BPh matrix, which were sufficiently small to be accommodated in the mesoporous cavity of COF-BPh, and the electronic effect of N atoms on Pd atoms and the confinement of COFs pores prompted the stable encapsulation of Pd clusters in the COF pores. Fig. 1d shows the high resolution TEM (HR-TEM) images of Pd@COF-BPh, further confirms that the Pd clusters are confined in the COF-BPh. The HR-TEM image (Fig. 1e) revealed that lattice fringes with a d spacing of 0.223 nm correspond to the Pd(111) plane [24,25]. The EDX element mapping clearly revealed a discrete distribution of C, N, and O and uniformly sized Pd clusters that are

highly dispersed in Pd@COF-BPh (Fig. 1f). In addition, Fig. S4 shows the TEM images of COF-Ph and Pd@COF-Ph. Pd clusters were highly dispersed in the COF-Ph layers, with particle sizes ranging from 0.2 to 1.2 nm, and the average particle size of Pd clusters is 0.79 nm. Figs. S5 and S6 show the EDX analysis results of Pd@COF-Ph and Pd@COF-BPh, respectively. Both catalysts contained H, C, N, and Pd. Table S1 summarizes the elemental composition and Pd content by ICP and EA analyses. The Pd loadings of Pd@COF-Ph and Pd@COF-BPh were 1.058% and 1.109%, respectively. By comparing the SEM and TEM analysis results of Pd@COF-Ph and Pd@COF-BPh, the Pd clusters were anchored in the pores with a similar size distribution. These phenomena clearly demonstrated that the micro-mesoporous nature of triazinyl-COF exhibits advantages of preventing the aggregation of Pd clusters.

N_2 adsorption analysis was carried out after the removal of the guest
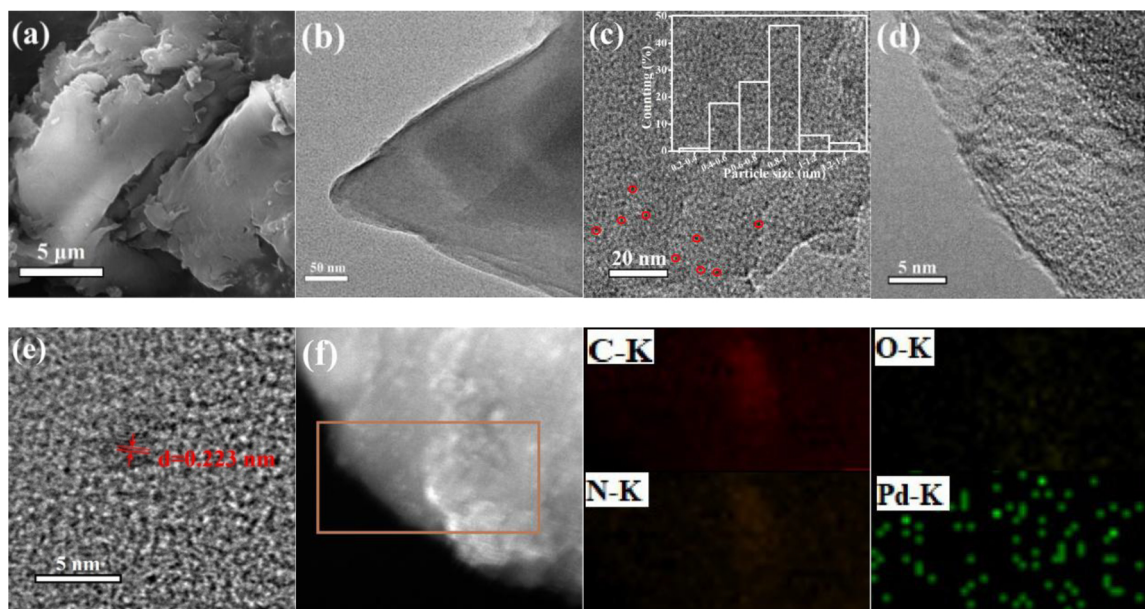

Fig. 1. SEM image of Pd@COF-BPh (a), low-magnification TEM images (b) and (c), high resolution TEM photos (d) and (e) of Pd@COF-BPh, (f) energy dispersive X-ray spectroscopy (EDX) mapping of composition element C, N, O and Pd, respectively.
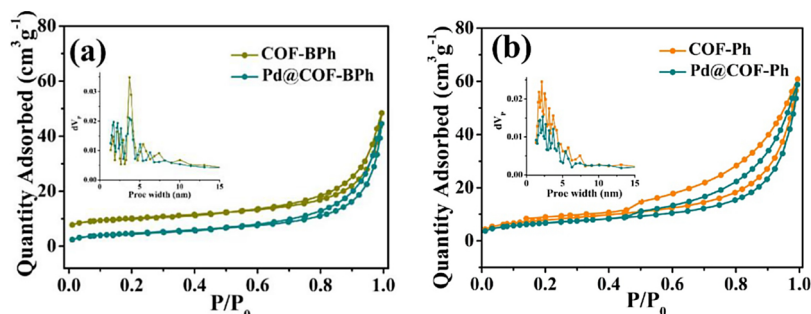
Fig. 2. N_2 adsorption−desorption isotherms and pore size distributions of (a) COF-BPh and Pd@COF-BPh, (b) COF-Ph and Pd@COF-Ph.
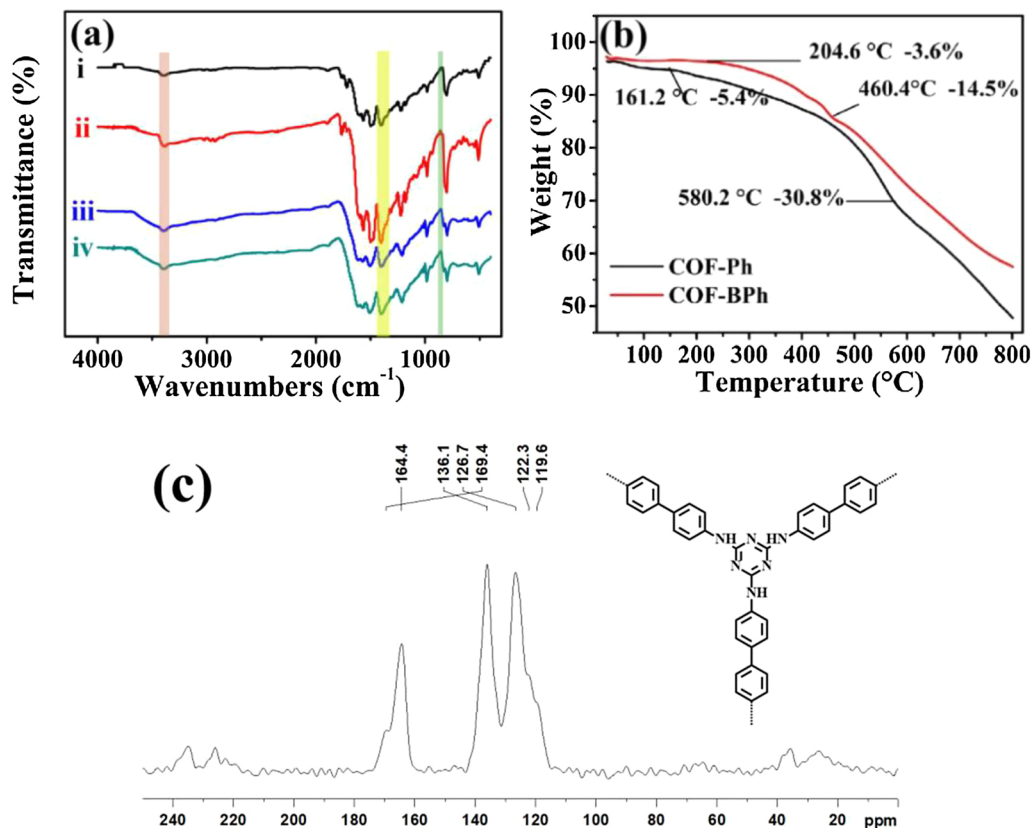

Fig. 3. (a) FT-IR spectra of the control sample COF-Ph (i), Pd@COF-Ph (ii), COF-BPh (iii), and Pd@COF-BPh (iv), (b) the TG analysis of COF-Ph and COF-BPh, (c) solid-state ^{13}C cross polarization (CP) NMR spectrum of COF-BPh with a spinning rate of 10 kHz.

molecules from the pores of the two COFs by vacuum activation. The N_2 isotherms of COF-BPh and Pd@COF-BPh (Fig. 2a) were measured at 77 K. A characteristic type IV isotherm, with an extremely small hysteresis loop, was observed. The isotherm exhibited a continuous increase at a high relative pressure ($0.4 < P/P_0 < 1.0$) with a hysteresis loop, indicative of its permanent mesoporous properties. Illustration in Fig. 2a shows the pore size distributions of COF-BPh and Pd@COF-BPh: Porosity was observed, with a predominantly large number of mesopores centered at ~3.8 nm and average pore diameters of 3.9 and 3.8 nm, respectively, and the aperture range from 1.4 to 9.6 nm was further confirmed. Owing to the size limitation effect, the average pore size (3.9 nm) in COF-BPh was greater than that of Pd clusters (0.2–1.4 nm), and the involved Pd clusters were located in the COF-BPh framework and stabilized by the triazinyl groups. Fig. 2b shows the nitrogen adsorption−desorption isotherms of COF-Ph and Pd@COF-Ph: A typical type IV isotherm was also observed, indicative of the dominance of mesopores. The pore size distributions of Pd@COF-Ph and COF-Ph ranged from 1.2 to 8 nm, and the average pore diameters were 2.3 and 2.25 nm, respectively. In addition, the specific surface areas of

Pd@COF-Ph and Pd@COF-BPh is 408 and 279 $m^2 g^{-1}$, respectively.

Fig. 3a shows the FTIR spectra of COF-Ph, COF-BPh, Pd@COF-Ph, and Pd@COF-BPh composites. The C−Cl stretching vibrations of cyanuric chloride at 848 cm^{-1} almost disappeared during the synthesis [26]. Meanwhile, vibration bands observed at 1302 cm^{-1} corresponded to the C−N stretching vibrations, indicative of the successful formation of both frameworks, and vibration bands observed at 3395 cm^{-1} corresponded to the N−H stretching vibrations [27,28]. COF-Ph and COF-BPh exhibited a negligible weight loss at a temperature less than 200 °C in the TGA curve (Fig. 3b), indicating that both catalysts exhibit good thermal stability and maintain a stable morphology during catalysis. The successful synthesis of COF-BPh is further confirmed by its solid-state ^{13}C cross-polarization NMR spectrum (Fig. 3c). The main peak centered at 164.4 ppm indicates most of cyanuric chloride (with a ^{13}C resonance peak of 169.4 ppm) had reacted with the 4,4′-diaminobiphenyl to form C−N single bond of the framework. And other aromatic ^{13}C NMR peaks at 136.1 ppm, 126.7 ppm, 122.3 ppm and 119.6 ppm show the fully embedding of 4,4′-diaminobiphenyl in the COF-BPh framework. The crystallinity of the COFs and Pd-cluster-modified COFs
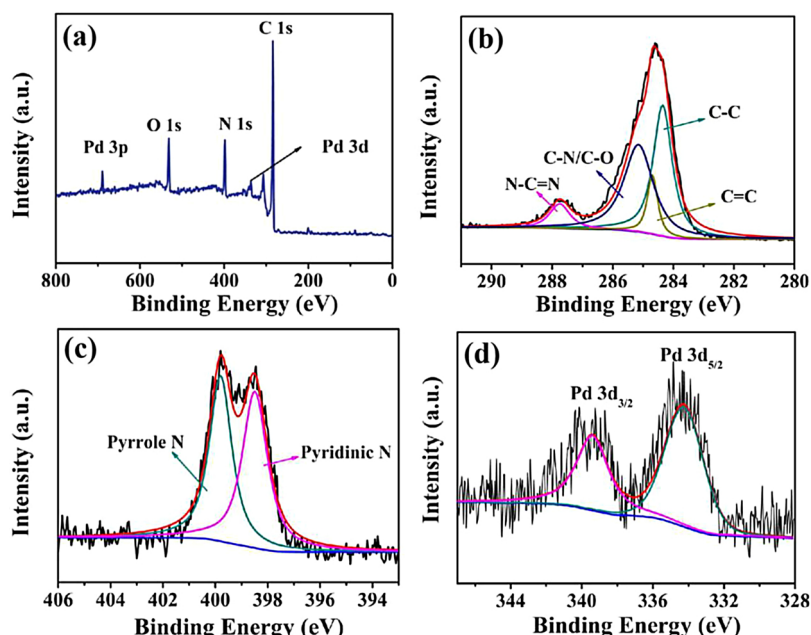
Fig. 4. The full-range XPS spectrum (a), and the narrow-range XPS spectra of C 1s (b), N 1s (c) and Pd 3d (d) of Pd@COF-BPh.
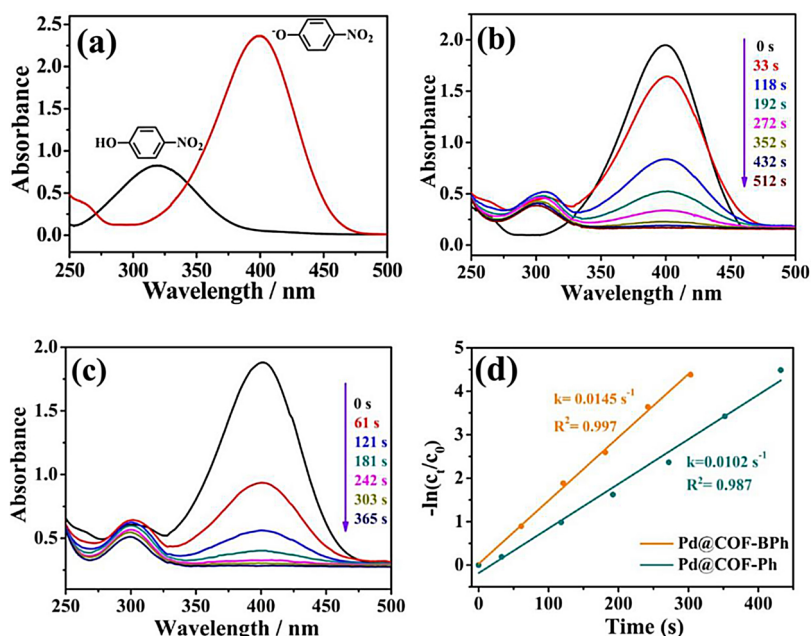

Fig. 5. UV–vis spectra of 4-NP before and after adding $NaBH_4$ solution (a), the successive reduction of 4-NP to 4-AP over the Pd@COF-Ph (b) and Pd@COF-BPh (c), pseudo-first order plots of 4-NP reduction catalyzed by Pd@COF-Ph and Pd@COF-BPh in the presence of $NaBH_4$ (d).

was confirmed by XRD analysis (Fig. S7), and the results indicated that the introduction of Pd clusters in the COFs pores by the DSM method does not change the crystallinity of the COFs. By the comparison of the standard card of Pd, characteristic peaks for Pd were not obviously observed in the XRD spectra of Pd@COF-Ph and Pd@COF-BPh, corresponding to the formation of extremely small clusters as well as low Pd contents [29].

XPS measurements were carried out to analyze the corresponding chemical bonding states of the Pd@COF-BPh and Pd@COF-Ph catalysts (Figs. 4 and S8, respectively). Fig. 4a shows the full-range XPS spectrum of the Pd@COF-BPh material: C 1s, N 1s, O 1s, Pd 3d, and Pd 3p components were observed. Fig. 4b–d represents the narrow-range XPS spectra of C, N, and Pd atoms. The deconvoluted high-resolution C 1s spectrum was divided into four distinct peaks, corresponding to C−C

(284.6 eV), C═C (284.8 eV), C−N/C−O (285.7 eV), and N−C═N (287.9 eV) in the triazine unit, respectively [30]. N 1s exhibited an extremely distinct peak, indicative of the higher content of N in Pd@COF-BPh. The EA result indicated a high N content of 21.13% for Pd@COF-BPh (Table S1). The XPS spectrum of N 1s was deconvoluted into two peaks at 398.6 and 399.7 eV, corresponding to pyridinic N and pyrroliz N, respectively [31]. Two strong peaks were observed at 334.6 and 339.9 eV in the high-resolution Pd 3d spectra, corresponding to Pd $3d_{5/2}$ and Pd $3d_{3/2}$, respectively. A peak corresponding to Pd^{2+} was not observed, indicating that Pd clusters exist as Pd^0. The deconvoluted peaks observed in the high-resolution spectra (Fig. S8b–d) of C 1s, N 1s and Pd 3d of Pd@COF-Ph were similar to those of Pd@COF-Ph with a high N content of 30.29%. In addition, the Pd clusters in Pd@COF-Ph was restored to Pd^0. Rich N atoms provided electrons to stabilize the Pd

Table 1
Comparison the catalytic performance for 4-NP reduction presented in literatures and the present work.

Entry	Catalysts	T (°C)	Time (min)	Pd (%)	K (min^{-1})	TOF (h^{-1})	Ref.
1	Pd@COF-Ph	25	8.53	1.058	0.612	212.3	this work
2	Pd@COF-BPh	25	6.08	1.109	0.87	284.1	this work
3	Pd@PC-POP	25	21.4	4.5	0.124	99.4	[34]
4	CNT/PiHP/Pd2	25	20	1.58	0.3	96	[35]
5	Pd NSs/CNNSs	25	6	1.2	0.76	169.16	[36]
6	Pd-GA/RGO	25	7	–	0.1199	–	[37]
7	Pd-Ni/C	25	8	–	0.160	–	[38]
8	Pd@TP-POP	25	5.75	1.31	0.61	227.07	[39]
9	Pd/NHPC	25	8	3.22	0.37	122.4	[40]
10	Pd-Ni/Fe$_3$O$_4$	25	11	2.6	0.2322	112.3	[41]
11	Au$_{1.0}$Pd$_{1.0}$	25	16	–	0.239	–	[42]
12	Ni@Pd/KCC-1	25	4.8	10.08	1.22	70.1	[43]
13	Pd/TiO$_2$	25	6	0.89	0.6	580	[44]
14	Pd-CeO$_2$	25	2	2.00	2.36	335	[45]
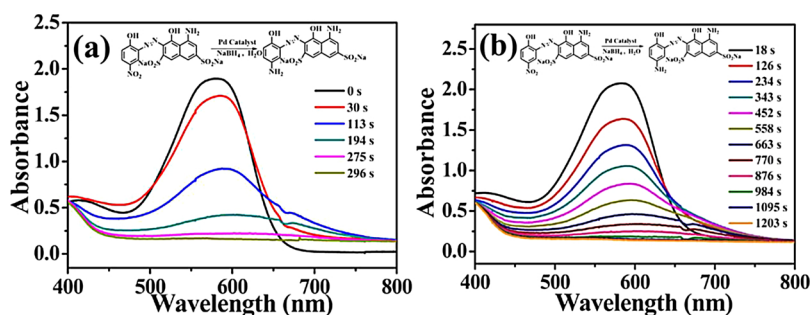
Fig. 6. UV–vis spectra of the catalytic process of MG-17 over Pd@COF-BPh (a) and Pd@COF-Ph (b).

Table 2
Exploring and optimizing the reaction conditions of reduction of nitrobenzene.[a]

Entry	Solvent	Catal. (mg)	Time (min)	Conv./Sel.[c]	TOF[d] (h^{-1})
1	H$_2$O/EtOH = 5/0(v/v)	Pd@COF-BPh (10)	60	74.5%/100%	707.9
2	H$_2$O/EtOH = 4/1(v/v)	Pd@COF-BPh (10)	60	92.5%/100%	880.5
3	H$_2$O/EtOH = 3/2(v/v)	Pd@COF-BPh (10)	25	98.5%/100%	2253.8
4	H$_2$O/EtOH = 1/1(v/v)	Pd@COF-BPh (10)	15	100%/100%	3807.5
5	H$_2$O/EtOH = 2/3(v/v)	Pd@COF-BPh (10)	15	94.7% /100%	3605.7
6	H$_2$O/EtOH = 1/4(v/v)	Pd@COF-BPh (10)	30	99.8%/100%	2374.8
7	H$_2$O/EtOH = 0/5(v/v)	Pd@COF-BPh (10)	30	77.7%/100%	1479.2
8	H$_2$O/EtOH = 1/1(v/v)	Pd@COF-BPh (5)	15	67.7%/100%	5155.4
9	H$_2$O/EtOH = 1/1(v/v)	Pd@COF-BPh (15)	10	100%/100%	3807.5
10	H$_2$O/EtOH = 1/1(v/v)	Pd@COF-Ph (10)	40	100%/100%	1508.8
11	H$_2$O/EtOH = 1/1(v/v)	COF-Ph (10)	60	0/0	0
12	H$_2$O/EtOH = 1/1(v/v)	COF-BPh (10)	60	0/0	0
13	H$_2$O/EtOH = 1/1(v/v)	none	60	0/0	0
14[b]	H$_2$O/EtOH = 1/1(v/v)	Pd@COF-BPh (10)	60	0/0	0

[a] Reaction conditions: 1 mmol nitrobenzene, 1.2 mmol NaBH$_4$, 25 °C.
[b] 1 mmol nitrobenzene, 25 °C.
[c] Catalytic reaction products were analyzed and identified by GC–MS.

clusters and prevent the leaching and sintering of Pd clusters.

3.2. Catalytic reduction of nitroaromatic compounds

Since the first report by Pal et al. for the reduction of 4-NP to 4-AP using a Ag catalyst in 2002 [32], this reaction became a model reaction; that is, a well-controlled reaction without the by-product formation for detecting the catalytic performance in an aqueous solution. The reduction of 4-NP in an aqueous-phase system in which NaBH$_4$ was used as the hydrogen source was selected to investigate and compare the catalytic efficiencies of Pd@COF-Ph and Pd@COF-BPh. The reaction

progress was monitored by changes in the absorption peaks, and the time-dependent absorption spectrum was recorded for the reduction of 4-NP over the Pd-cluster-loaded catalysts (Fig. 5). With the addition of NaBH$_4$ to form 4-nitrophenolate ions, the initial absorption peak for 4-NP was observed at a λ of 317 nm, the solution turned bright yellow, and the absorption peak shifted to 400 nm (Fig. 5a). However, with the introduction of the catalysts into the reaction mixture, the absorption peak gradually decreased at a λ of 400 nm, while that of 4-AP at a λ of 300 nm increased as 4-AP was the sole product. Fig. 5b–c show the UV–vis spectra of the catalytic process of 4-NP over Pd@COF-Ph and Pd@COF-BPh. Catalytic reduction over Pd@COF-BPh was completed in

Table 3
Reaction results of reduction of various R-NO$_2$ compounds by Pd@COF-BPh.[a]

$$R-\text{C}_6\text{H}_4-NO_2 \xrightarrow[\text{H}_2\text{O/EtOH}=1/1,\ 25^\circ\text{C}]{\text{NaBH}_4,\ \text{Pd@COF-BPh}} R-\text{C}_6\text{H}_4-NH_2$$

Entry	Substrate	Product	Yield (%)[c]	TOF (h^{-1})[d]
1	nitrobenzene	aniline	> 99%	3807.5
2	4-Cl-nitrobenzene	4-Cl-aniline	> 99%	3807.5
3	3-Cl-nitrobenzene	3-Cl-aniline	> 99%	3807.5
4	2-Cl-nitrobenzene	2-Cl-aniline	> 99%	3807.5
5	di-Cl-nitrobenzene	di-Cl-aniline	> 99%	3807.5
6	Br-nitrobenzene	Br-aniline	> 99%	3807.5
7	2-Br-nitrobenzene	2-Br-aniline	> 99%	3807.5
8	HO-nitrobenzene	HO-aniline	> 99%	3807.5
9	OH-nitrobenzene	OH-aniline	> 99%	3807.5
10	H$_2$N-nitrobenzene	H$_2$N-aniline	> 99%	3807.5
11	NH$_2$-nitrobenzene	NH$_2$-aniline	> 99%	3807.5
12	NH$_2$-nitrobenzene	NH$_2$-aniline	> 99%	3807.5
13	H$_3$C-nitrobenzene	H$_3$C-aniline	> 99%	3807.5
14	CH$_3$-nitrobenzene	CH$_3$-aniline	77.4%	3217.2
15[b]	O$_2$N-dinitrobenzene	H$_2$N-diaminobenzene	78.4%	2985.1
16[b]	NO$_2$-dinitrobenzene	NH$_2$-diaminobenzene	> 99%	3807.5

[a] Reaction conditions: 1 mmol substrate, 1.2 mmol NaBH$_4$, 25 °C, 10 mg Pd@COF-BPh catalyst, 2.5 mL of EtOH, 2.5 mL of H$_2$O.
[b] 1 mmol substrate, 2.4 mmol NaBH$_4$, 25 °C, 10 mg Pd@COF-BPh catalyst, 2.5 mL of EtOH, 2.5 mL of H$_2$O.
[c] Catalytic reaction products were analyzed and identified by GC–MS.

Fig. 7. The recyclability of Pd@COF-Ph and Pd@COF-BPh.

~365 s, while Pd@COF-Ph required a longer reaction time (512 s). This reduction process was considered to be a pseudo-first-order reaction [32,33]. Hence, the kinetic constants for the Pd@COF-Ph and Pd@COF-BPh catalysts are evaluated according to the slope $\ln(c_t/c_0) = -kt$ in the linear range. Fig. 5d shows the result. The k values for Pd@COF-BPh and Pd@COF-Ph were 0.0145 s^{-1} and 0.0102 s^{-1}, respectively.

Notably, the catalytic activities of Pd@COF-Ph and Pd@COF-BPh were significantly better than those of several reported Pd-based catalysts, and the k values were greater than those at the same loading (Table 1) [34–45]. Combining the characterization results of both Pd@COF-Ph and Pd@COF-BPh catalysts, the reasons for their superior catalytic performance were follows: First, from the TEM analysis, the highly dispersed, ultrafine Pd nanoclusters confined in the COFs pores have a positive effect on improving the atomic utilization of the Pd active sites as compared with other Pd NPs based catalysts. Second, the Pd clusters confined in the COFs pores are not easy to agglomerated and sintered. Third, high specific surface areas and micro-mesoporous structures of the COF supports are beneficial to the adsorption of reactants, and the abundant micro-mesopores provide convenient
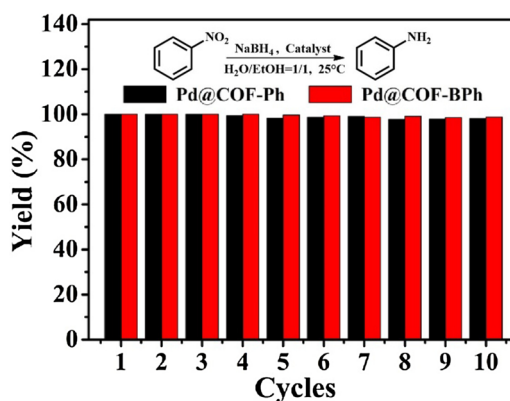
condition for mass transfer of reactants. All the above reasons are the main factors for the high activity of Pd@COF-Ph and Pd@COF-BPh catalysts. Besides, the Pd@COF-BPh catalyst has more excellent catalytic activity than Pd@COF-Ph catalyst under the same reaction conditions, mainly due to Pd@COF-BPh and Pd@COF-Ph have different average pore size distribution of 3.8 nm and 2.25 nm, respectively. Which leads to the difference in the catalytic performance of the two catalysts.

In order to investigate the effect of the different pore size on catalytic activity between Pd@COF-BPh and Pd@COF-Ph, we further chose the catalytic reduction of MG-17 with large molecule size (7.2 Å × 14.0 Å) as a probe reaction in aqueous solution (Fig. S1). The Pd@COF-BPh exhibits excellent catalytic activity and the reduction of MG-17 can be completed in 5 min (Fig. 6a). Instead, the Pd@COF-Ph with a smaller pore size cannot promote the reduction of MG-17 and the reaction time extends to 20 min (Fig. 6b), the main reason of which is that the molecular size of MG-17 is close to the pore size of COF-Ph, and the mass transfer process is slow. Therefore, Pd@COF-BPh exhibits better catalytic activity, owing to the better mass transfer of porous COF-BPh material with a larger pore size than that of the Pd@COF-Ph catalyst.

As the Pd@COF-BPh catalyst exhibited better performance than the Pd@COF-Ph catalyst, the general applicability of Pd@COF-BPh for the catalytic reduction of nitroarenes was investigated in detail. By using nitrobenzene as a model compound, a certain amount of NaBH$_4$ was added to a flask containing nitrobenzene and the Pd@COF-BPh catalyst solution to initiate the reaction. Table 2 summarizes the reaction conditions. First, the composition of the reaction solvent was examined (Table 2, entries 1–7). At the same dosage of the Pd@COF-BPh catalyst, with the increase in the proportion of ethanol in the reaction solvent, the conversion of nitrobenzene increased, related to the better dispersibility of the catalyst in ethanol and the higher solubility of nitrobenzene. At a H$_2$O/EtOH content of 1/1(v/v), the reaction was completed in only 15 min, and a high TOF value of 3807.5 h^{-1} was obtained. Under optimal solvent conditions, the effect of the amount of the Pd@COF-BPh catalyst on the reaction was examined (entries 8–9, Table 2). From the experimental results, the reaction conversion increases with the catalyst amount. By using 15 mg of Pd@COF-BPh, the reaction was completed in only 10 min, and the TOF value was the same as that shown in entry 4. Under the same reaction conditions, the catalytic activity of Pd@COF-Ph was also compared (Table 2, entry 10): The reaction time was extended to 40 min, and the TOF value was 1508.8 h^{-1}, further confirming that the catalytic activity of Pd@COF-BPh is better than that of Pd@COF-Ph. The reduction of nitrobenzene did not occur over the COF-Ph and COF-BPh catalysts (entries 11–12, Table 2, respectively), and the reaction did not proceed without catalysts (entry 13, Table 2). These results indicated that Pd clusters are the main active sites for the reduction of nitro compounds. In the absence of NaBH$_4$ (Table 2, entry 14), the reaction also did not proceed.

With the optimized reaction conditions, various nitroarenes examined at room temperature were converted to the corresponding amines with an excellent yield. In case of nitro compounds with monosubstituted or disubstituted halogens at different positions of nitrobenzene, excellent yields were obtained (> 99%), and dehalogenation did not occur, which is crucial for industrial applications because halogenated anilines are key intermediates for fine chemicals, and dehalogenated by-products exhibit a corrosive effect on the equipment, limiting its industrial applications (Table 3, entries 1–7). Various aromatic nitro compounds with an electron-rich group were efficiently reduced in the same manner. For example, nitrobenzene with p-hydroxy, o-hydroxy, o-amino, m-amino, p-amino, o-methyl, and p-methyl groups was reduced to the corresponding amine products in 15 min under the same conditions (entries 8–14, Table 3). In particular, 2,4-dinitroaniline and 2,4-dinitrobenzene were converted to 1,2,4-trianiline and 2,4-dianiline, respectively, with 100% selectivity (entries 15–16, Table 3). All of the experimental results revealed that nitroaromatic compounds containing electron-donating and electron-withdrawing substituents can be converted into the corresponding amine compounds over the Pd@COF-BPh catalyst. The substituent exhibited a large effect on the reaction because the substituent inactivated the nitro group, leading to the decreased conversion of the nitro group. In addition, different substituents exhibited different effects. A majority of the nitro compounds in Table 3 exhibited extremely good conversion and selectivity, indicating that the Pd@COF-BPh catalyst exhibits good applicability. In addition, the Pd@COF-Ph catalyst exhibited good performance for the reduction of various aromatic nitro compounds, and Table S2 summarizes the results obtained.

Stability and reusability are the most important indicators for evaluating the catalytic performance. After 10 consecutive runs, the conversion negligibly decreased (Fig. 7). The Pd content of the recovered catalysts was almost unchanged, indicating that almost no leaching of the active site occurs during the reaction (Table S1). The TEM images of recovered Pd@COF-Ph and Pd@COF-BPh indicated that there is no clear agglomeration of the Pd clusters, and the average particle size is still ~0.8 nm (Fig. S9). Hence, the synthetic strategy for Pd-cluster-modified catalysts in this study can effectively improve the stability of noble-metal clusters, prevent their aggregation and loss, and provide assistance for the synthesis and application of noble-metal-cluster catalysts.

4. Conclusions

In summary, two triazinyl-COFs with different pore sizes were designed. According to the electronic effect of N atoms on Pd atoms and the confinement of COF pores, Pd clusters were confined into COF pores by a simple double solvent method, affording two Pd clusters catalysts Pd@COF-Ph and Pd@COF-BPh with different pore sizes, respectively. Compared to other noble metal-based catalysts, the as-obtained catalysts exhibited excellent activity for the reduction of nitroarenes. The Pd@COF-BPh catalyst with larger pores exhibited greater activity than that of the Pd@COF-Ph catalyst due to the pore size effect of the supports. This study exhibits certain positive effects for the development of stable, highly dispersed noble-metal-cluster-based catalysts.

Conflicts of interest

There are no conflicts to declare.

Acknowledgement

Appendix A. Supplementary data

Supplementary material related to this article can be found, in the online version, at doi:https://doi.org/10.1016/j.apcatb.2019.117942.

References

[1] E.L. Margelefsky, R.K. Zeidan, M.E. Davis, Cooperative catalysis by silica-supported organic functional groups, Chem. Soc. Rev. 37 (2008) 1118–1126.

[2] J. Zhang, X. Han, X. Wu, Y. Liu, Y. Cui, Multivariate chiral covalent organic frameworks with controlled crystallinity and stability for asymmetric catalysis, J. Am. Chem. Soc. 139 (2017) 8277–8285.

[3] Alexandre F. Trindade, Pedro M.P. Gois, Carlos A.M. Afonso, Recyclable stereoselective catalysts, Chem. Rev. 109 (2009) 418–514.

[4] D. Wang, D. Astruc, Fast-growing field of magnetically recyclable nanocatalysts, Chem. Rev. 114 (2014) 6949–6985.

[5] M. Bhadra, H.S. Sasmal, A. Basu, S.P. Midya, S. Kandambeth, P. Pachfule, E. Balaraman, R. Banerjee, Predesigned metal-anchored building block for in situ generation of Pd nanoparticles in porous covalent organic framework: application in heterogeneous tandem catalysis, ACS Appl. Mater. Interfaces 9 (2017) 13785–13792.

[6] D. Astruc, F. Lu, J.R. Aranzaes, Nanoparticles as recyclable catalysts: the frontier between homogeneous and heterogeneous catalysis, Angew. Chem. 44 (2005) 7852–7872.

[7] A.M. Argo, J.F. Odzak, F.S. Lai, B.C. Gates, Observation of ligand effects during alkene hydrogenation catalysed by supported metal clusters, Nature 415 (2002) 623–626.

[8] N. Wang, Q. Sun, R. Bai, X. Li, G. Guo, J. Yu, In situ confinement of ultrasmall Pd clusters within nanosized silicalite-1 zeolite for highly efficient catalysis of hydrogen generation, J. Am. Chem. Soc. 138 (2016) 7484–7487.

[9] Tetsuro Murahashi, Mayu Fujimoto, Hideo Kurosawa, Discrete sandwich compounds of monolayer palladium sheets, Science 313 (2006) 1104–1107.

[10] A. Leyva-Perez, J. Oliver-Meseguer, P. Rubio-Marques, A. Corma, Water-stabilized three- and four-atom palladium clusters as highly active catalytic species in ligand-free C-C cross-coupling reactions, Angew. Chem. Int. Ed. 52 (2013) 11554–11559.

[11] P. Serna, B.C. Gates, Molecular metal catalysts on supports: organometallic chemistry meets surface science, Acc. Chem. Res. 47 (2014) 2612–2620.

[12] R. Schimmenti, R. Cortese, D. Duca, M. Mavrikakis, Boron nitride-supported subnanometer Pd$_6$ clusters for formic acid decomposition: a DFT study, ChemCatChem 9 (2017) 1610–1620.

[13] L. Liu, U. Diaz, R. Arenal, G. Agostini, P. Concepcion, A. Corma, Generation of subnanometric platinum with high stability during transformation of a 2D zeolite into 3D, Nat. Mater. 16 (2017) 132–138.

[14] F.R. Fortea-Perez, M. Mon, J. Ferrando-Soria, M. Boronat, A. Leyva-Perez, A. Corma, J.M. Herrera, D. Osadchii, J. Gascon, D. Armentano, E. Pardo, The MOF-driven synthesis of supported palladium clusters with catalytic activity for carbene-mediated chemistry, Nat. Mater. 16 (2017) 760–766.

[15] B.C. Gates, Supported metal clusters: synthesis, structure, and catalysis, Chem. Rev. 95 (1995) 511–522.

[16] N. Huang, P. Wang, D. Jiang, Covalent organic frameworks: a materials platform for structural and functional designs, Nat. Rev. Mater. 1 (2016) 1–19.

[17] B.P. Biswal, S. Chandra, S. Kandambeth, B. Lukose, T. Heine, R. Banerjee, Mechanochemical synthesis of chemically stable isoreticular covalent organic frameworks, J. Am. Chem. Soc. 135 (2013) 5328–5331.

[18] T.Y. Zhou, S.Q. Xu, Q. Wen, Z.F. Pang, X. Zhao, One-step construction of two different kinds of pores in a 2D covalent organic framework, J. Am. Chem. Soc. 136 (2014) 15885–15888.

[19] D. Wu, F. Xu, B. Sun, R. Fu, H. He, K. Matyjaszewski, Design and preparation of porous polymers, Chem. Rev. 112 (2012) 3959–4015.

[20] S.Y. Ding, W. Wang, Covalent organic frameworks (COFs): from design to applications, Chem. Soc. Rev. 42 (2013) 548–568.

[21] S. Lu, Y. Hu, S. Wan, R. McCaffrey, Y. Jin, H. Gu, W. Zhang, Synthesis of ultrafine and highly dispersed metal nanoparticles confined in a thioether-containing covalent organic framework and their catalytic applications, J. Am. Chem. Soc. 139 (2017) 17082–17088.

[22] C.E. Chan-Thaw, A. Villa, P. Katekomol, D. Su, A. Thomas, L. Prati, Covalent triazine framework as catalytic support for liquid phase reaction, Nano Lett. 10 (2010) 537–541.

[23] R. McCaffrey, H. Long, Y. Jin, A. Sanders, W. Park, W. Zhang, Template synthesis of gold nanoparticles with an organic molecular cage, J. Am. Chem. Soc. 136 (2014) 1782–1785.

[24] X. Xu, M. Tang, M. Li, H. Li, Y. Wang, Hydrogenation of benzoic acid and derivatives over Pd nanoparticles supported on N-doped carbon derived from glucosamine hydrochloride, ACS Catal. 4 (2014) 3132–3135.

[25] Z. Chen, Y. Liang, D.-S. Jia, Z.-M. Cui, W.-G. Song, Simple synthesis of sub-nanometer Pd clusters: high catalytic activity of Pd/PEG-PNIPAM in Suzuki reaction, Chin. J. Catal. 38 (2017) 651–657.

[26] H.-C. Ma, J.-L. Kan, G.-J. Chen, C.-X. Chen, Y.-B. Dong, Pd NPs-loaded homochiral covalent organic framework for heterogeneous asymmetric catalysis, Chem. Mater. 29 (2017) 6518–6524.

[27] G.Y. Lee, J. Lee, H.T. Vo, S. Kim, H. Lee, T. Park, Amine-functionalized covalent organic framework for efficient SO$_2$ capture with high reversibility, Sci. Rep. 7 (2017) 557.

[28] S. Kandambeth, V. Venkatesh, D.B. Shinde, S. Kumari, A. Halder, S. Verma,

R. Banerjee, Self-templated chemically stable hollow spherical covalent organic framework, Nat. Commun. 6 (2015) 6786.

[29] A. Aijaz, A. Karkamkar, Y.J. Choi, N. Tsumori, E. Ronnebro, T. Autrey, H. Shioyama, Q. Xu, Immobilizing highly catalytically active Pt nanoparticles inside the pores of metal-organic framework: a double solvents approach, J. Am. Chem. Soc. 134 (2012) 13926–13929.

[30] X. Cui, K. Liang, M. Tian, Y. Zhu, J. Ma, Z. Dong, Cobalt nanoparticles supported on N-doped mesoporous carbon as a highly efficient catalyst for the synthesis of aromatic amines, J. Colloid Interface Sci. 501 (2017) 231–240.

[31] T. Sun, L. Xu, S. Li, W. Chai, Y. Huang, Y. Yan, J. Chen, Cobalt-nitrogen-doped ordered macro-/mesoporous carbon for highly efficient oxygen reduction reaction, Appl. Catal. B: Environ. 193 (2016) 1–8.

[32] N. Pradhan, A. Pal, T. Pal, Silver nanoparticle catalyzed reduction of aromatic nitro compounds, Colloids Surf. A 196 (2002) 247–257.

[33] R. Yan, Y. Zhao, H. Yang, X.-J. Kang, C. Wang, L.-L. Wen, Z.-D. Lu, Ultrasmall Au nanoparticles embedded in 2D mixed-ligand metal-organic framework nanosheets exhibiting highly efficient and size-selective catalysis, Adv. Funct. Mater. 28 (2018) 1802021.

[34] M. Yuan, R. Yang, S. Wei, X. Hu, D. Xu, J. Yang, Z. Dong, Ultra-fine Pd nanoparticles confined in a porous organic polymer: a leaching-and-aggregation-resistant catalyst for the efficient reduction of nitroarenes by NaBH₄, J. Colloid Interface Sci. 538 (2019) 720–730.

[35] H. Li, L. Han, J. Cooper-White, I. Kim, Palladium nanoparticles decorated carbon nanotubes: facile synthesis and their applications as highly efficient catalysts for the reduction of 4-nitrophenol, Green Chem. 14 (2012) 586–591.

[36] K. Gu, X. Pan, W. Wang, J. Ma, Y. Sun, H. Yang, H. Shen, Z. Huang, H. Liu, In situ growth of Pd nanosheets on g-C₃N₄ nanosheets with well-contacted interface and enhanced catalytic performance for 4-nitrophenol reduction, Small (2018) e1801812.

[37] A.T.E. Vilian, S.R. Choe, K. Giribabu, S.C. Jang, C. Roh, Y.S. Huh, Y.K. Han, Pd nanospheres decorated reduced graphene oxide with multi-functions: highly efficient catalytic reduction and ultrasensitive sensing of hazardous 4-nitrophenol pollutant, J. Hazard. Mater. 333 (2017) 54–62.

[38] T.A. Revathy, S. Dhanavel, T. Sivaranjani, V. Narayanan, T. Maiyalagan, A. Stephen, Highly active graphene-supported palladium-nickel alloy nanoparticles for catalytic reduction of 4-nitrophenol, Appl. Surf. Sci. 449 (2018) 764–771.

[39] J. Yang, M. Yuan, D. Xu, H. Zhao, Y. Zhu, M. Fan, F. Zhang, Z. Dong, Highly dispersed ultrafine palladium nanoparticles encapsulated in a triazinyl functionalized porous organic polymer as a highly efficient catalyst for transfer hydrogenation of aldehydes, J. Mater. Chem. A 6 (2018) 18242–18251.

[40] X.X. Wu, H. Zhou, Hierarchical porous N-doped carbon supported palladium (Pd/NHPC) as a sustainable catalyst for the reduction of 4-nitrophenol with good activity and lifetime, New J. Chem. 41 (2017) 10245–10250.

[41] N. Ghanbari, S.J. Hoseini, M. Bahrami, Ultrasonic assisted synthesis of palladium-nickel/iron oxide core-shell nanoalloys as effective catalyst for Suzuki-Miyaura and p-nitrophenol reduction reactions, Ultrason. Sonochem. 39 (2017) 467–477.

[42] G. Han, X. Li, J. Li, X. Wang, Y.S. Zhang, R. Sun, Special magnetic catalyst with lignin-reduced Au–Pd nanoalloy, ACS Omega 2 (2017) 4938–4945.

[43] Z. Dong, X. Le, C. Dong, W. Zhang, X. Li, J. Ma, Ni@Pd core–shell nanoparticles modified fibrous silica nanospheres as highly efficient and recoverable catalyst for reduction of 4-nitrophenol and hydrodechlorination of 4-chlorophenol, Appl. Catal. B: Environ. 162 (2015) 372–380.

[44] M. Imran, A.B. Yousaf, X. Zhou, Y.-F. Jiang, C.-Z. Yuan, A. Zeb, N. Jiang, A.-W. Xu, Pd/TiO₂ nanocatalyst with strong metal–support interaction for highly efficient durable heterogeneous hydrogenation, J. Phys. Chem. C 121 (2017) 1162–1170.

[45] C. Du, Y. Guo, Y. Guo, X.-q. Gong, G. Lu, Polymer-templated synthesis of hollow Pd–CeO₂ nanocomposite spheres and their catalytic activity and thermal stability, J. Mater. Chem. A 3 (2015) 23230–23239.

Update

Applied Catalysis B: Environmental

Corrigendum to "Palladium clusters confined in triazinyl-functionalized COFs with enhanced catalytic activity" [Appl. Catal. B: Environ. 257 (2019) 117942]

Mengying Fan[a], Wei David Wang[a], Yangyang Zhu[a], Xun Sun[b,*], Fengwei Zhang[c,*], Zhengping Dong[a,*]

[a] State Key Laboratory of Applied Organic Chemistry, Laboratory of Special Function Materials and Structure Design of the Ministry of Education, College of Chemistry and Chemical Engineering, Lanzhou University, Lanzhou 730000, PR China
[b] Shandong Applied Research Center of Gold Nanotechnology (Au-SDARC), School of Chemistry & Chemical Engineering, Yantai University, Yantai 264005, PR China
[c] Institute of Crystalline Materials, Shanxi University, Taiyuan 030006, PR China

The authors deeply regret to inform that the aforementioned article contains some errors.

We are deeply sorry since we realized the errors just after we carefully checked the online PDF version of the article.

(1) The formula of the right superscript "d" in Tables 2 and 3 is missing in the PDF version of the article.

Table 2 Exploring and optimizing the reaction conditions of reduction of nitrobenzene.[a]
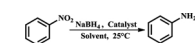
Entry	Solvent	Catal. (mg)	Time (min)	Conv.[c]/ Sel.	TOF[d] (h^{-1})
1	H$_2$O/EtOH = 5/0(v/v)	Pd@COF-BPh (10)	60	74.5%/ 100%	707.9
…	…	…	…	…	…
…	…	…	…	…	…

[a] Reaction conditions: 1 mmol nitrobenzene, 1.2 mmol NaBH$_4$, 25 °C.
[b] 1 mmol nitrobenzene, 25 °C.
[c] Catalytic reaction products were analyzed and identified by GC–MS.
[d] $\text{TOF} = \frac{\text{moles of converted substrate}}{\text{moles of Pd} \times \text{reaction time (h)}}$.

Table 3 Reaction results of reduction of various R-NO$_2$ compounds by Pd@COF-BPh.[a]

Entry	Substrate	Product	Yield[c] (%)	TOF[d] (h^{-1})
1			> 99%	3807.5
…	…	…	…	…
…	…	…	…	…

[a] Reaction conditions: 1 mmol substrate, 1.2 mmol NaBH$_4$, 25 °C, 15 min, 10 mg Pd@COF-BPh catalyst, 2.5 mL of EtOH, 2.5 mL of H$_2$O.
[b] 1 mmol substrate, 2.4 mmol NaBH$_4$, 25 °C, 15 min, 10 mg Pd@COF-BPh catalyst, 2.5 mL of EtOH, 2.5 mL of H$_2$O.
[c] Catalytic reaction products were analyzed and identified by GC–MS.
[d] $\text{TOF} = \frac{\text{moles of converted substrate}}{\text{moles of Pd} \times \text{reaction time (h)}}$.

(2) In Page 4 of the PDF article version. We deeply apologize for our clerical mistake to wrongly type and miss the decimal point of the specific surface areas numbers of the Pd@COF-Ph and Pd@COF-BPh catalysts.

The sentence in Page 4: "**In addition, the specific surface areas of Pd@COF-Ph and Pd@COF-BPh is 408 and 279 m^2 g^{-1}, respectively.**" should be corrected to "**In addition, the specific surface areas of Pd@COF-Ph and Pd@COF-BPh is 40.8 and 27.9 m^2 g^{-1}, respectively.**". These corrections do not change the overall results & discussion, and conclusion reported in the published article.

Authors deeply apologize for the inconvenience caused.